JACS
JOURNAL OF THE AMERICAN CHEMICAL SOCIETY
Communication
pubs.acs.org/JACS
Terms of Use

Influence of Side-Chain Regiochemistry on the Transistor Performance of High-Mobility, All-Donor Polymers

Zhuping Fei,[†] Pichaya Pattanasattayavong,[‡] Yang Han,[†] Bob C. Schroeder,[†] Feng Yan,[§] R. Joseph Kline,[∥] Thomas D. Anthopoulos,[‡] and Martin Heeney*[,†]

[†]Department of Chemistry and Centre for Plastic Electronics, Imperial College London, Exhibition Road, London SW7 2AZ, U.K.
[‡]Department of Physics and Centre for Plastic Electronics, Imperial College London, Exhibition Road, London SW7 2AZ, U.K.
[§]Department of Applied Physics and Materials Research Centre, The Hong Kong Polytechnic University, Hung Hom, Kowloon, Hong Kong
[∥]National Institute of Standards and Technology, Gaithersburg, Maryland 20899, United States

Supporting Information

ABSTRACT: Three novel polythiophene isomers are reported whereby the only difference in structure relates to the regiochemistry of the solubilizing side chains on the backbone. This is demonstrated to have a significant impact on the optoelectronic properties of the polymers and their propensity to aggregate in solution. These differences are rationalized on the basis of differences in backbone torsion. The polymer with the largest effective conjugation length is demonstrated to exhibit the highest field-effect mobility, with peak values up to 4.6 $cm^2\ V^{-1}\ s^{-1}$.

Solution-processed polymer organic semiconductors have attracted wide attention due to their potential for use in next-generation flexible and low-cost electronic devices. The use of such polymers as the active semiconducting component in organic field effect transistors is one interesting application. One of the key parameters for such transistors is the charge carrier mobility. In the past few years there have been impressive increases in charge carrier mobility reported for certain classes of organic polymers, with average p-type mobilities of 9−12 $cm^2\ V^{-1}\ s^{-1}$ now reported for devices fabricated from simple solution-casting techniques like spin-coating.[1] Higher mobilities have also been reported for polymers processed by special techniques to increase the alignment of the polymer chains or improve ordering.[2] Most of these polymers have a donor−acceptor (D−A)-type structure, where electron-rich and electron-poor co-monomers are polymerized to give a small optical band gap.[3] In some cases such small band gaps are undesirable, since they can result in ambipolar behavior, making it difficult to turn the device off,[4] or result in electrical characteristics which show strong deviations from ideal behavior.[5]

The charge-transport behavior of wider band gap, all-donor polymers has yet to match the performance of these newer classes of low band gap polymer and is typified by thiophene-rich semicrystalline polymers like poly(2,5-bis(3-alkylthiophen-2-yl)thieno[3,2-*b*]thiophene) (pBTTT)[6] or poly[5,5′-bis(3-alkyl-2-thienyl)-2,2′-bithiophene][7] (pQT), with mobilities around 0.1−1 $cm^2\ V^{-1}\ s^{-1}$. Although such polymers form thin films with high degrees of lamellar order by ordering of the side chains,[8] the factor limiting charge transport has been suggested to be paracrystalline disorder in the π-stacking direction, which leads to a charge trapping.[9] Interestingly, in the case of D−A polymers, there is often no evidence for any long-range order, and instead the high mobility appears related to the polymers' ability to form aggregates with short-range order at the segmental level.[9,10] At a molecular level this can be related to the relatively rigid polymer backbone in many instances, as a result of the rigid, fused aromatic monomers or the low-lying LUMO level, which promotes backbone quinoidal character.

The origin of the paracrystalline disorder in pBTTT and related polythiophenes is not yet clear, but we theorized that torsional disorder along the backbone caused by the steric interactions of the 3-alkylthiophene with the adjacent thieno[3,2-*b*]thiophene might be a contributory cause. In order to try to reduce the torsional disorder along the backbone, we reasoned that the introduction of vinylene linker group could help to reduce steric interactions and increase conjugation length. In order to probe this, we designed three isomeric all-donor co-polymers whereby the positions of solubilizing alkyl chains on the conjugated backbone was systematically altered (Figure 1), such that they were contained on the rigid thieno[3,2-*b*]thiophene (**P1**), on the bithiophene but adjacent to the thienothiophene (**P2**), or adjacent to the vinylene linker (**P3**). Here we demonstrate that the placement of the side chains has a

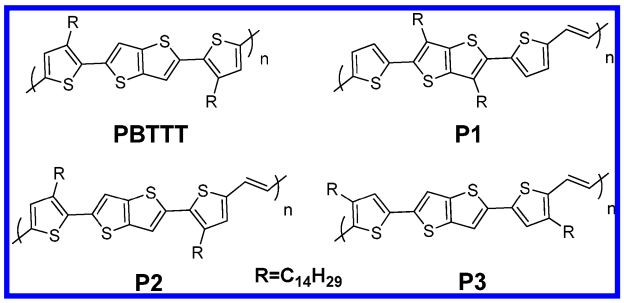

Figure 1. Structures of poly(2,5-bis(3-tetradecylthiophen-2-yl)thieno-[3,2-*b*]thiophene) [pBTTT] and vinylene co-polymers **P1**−**P3**.

Received: August 31, 2014
Published: October 10, 2014

Table 1. Molecular Weights, Optical Properties, and Experimental and Calculated Energy Levels of P1−P3

	M_n[a] (kDa)	M_w[a] (kDa)	Đ[a]	λ_{max} (nm), soln	λ_{max} (nm), film	HOMO[b] (eV)	DFT HOMO/LUMO (eV)	$E_{g,opt}$[c] (eV)	$E_{g,calc}$ (eV)
P1	29	69	2.6	497	538	−5.11	−4.69/−2.60	1.97	2.09
P2	26	86	3.3	503	553	−5.08	−4.70/−2.58	1.88	2.12
P3	20	58	2.9	552	586, 631	−4.97	−4.51/−2.70	1.78	1.81

[a]Determined by GPC and reported as their polystyrene equivalents. [b]Determined as a thin film by UV-PESA. [c]Determined by onset of optical absorption of thin film.

significant impact of the conjugation length of the polymer and the performance in field-effect transistors (FETs), with **P3** exhibiting charge carrier mobilities up to 4.6 $cm^2\ V^{-1}\ s^{-1}$. We rationalize the differences on the basis of different degrees of backbone torsion, depending of the regiochemistry of the alkyl side chains.

The synthesis of **P1−P3** is shown in Scheme S1. All polymers were synthesized by Stille polymerization between the appropriate dibrominated thiophene monomer and *trans*-1,2-bis(tributylstannyl)ethylene. Monomers **M1−M3** were synthesized as shown in Scheme S1, following standard cross-coupling routes. The synthesis of 3,6-ditetradecylthieno[3,2-*b*]thiophene is worth highlighting, since it is a substantial simplification over the previously reported routes.[11] Here the alkyl chains were introduced by Negishi cross-coupling of 3,6-dibromothieno[3,2-*b*]thiophene with tetradecylzinc chloride in the presence of $Pd(dpppf)Cl_2$ under microwave heating. The reaction only proceeded at appreciable rate under high temperature, and 10 min at 150 °C was found to be optimum. The crude product was brominated directly before purification, since the product **2** was readily crystallized, to give a yield of 45% over the two steps.

The polymerizations were all performed under microwave heating, and the crude polymers were purified by precipitation and Soxhlet extraction to remove low-weight oligomers and catalyst residues. Following extraction and precipitation the final polymers, **P1−P3** were obtained as dark brown solids in yields of 67%, 41%, and 61%, respectively. **P1** and **P2** could be readily dissolved in common solvents such as chloroform, THF, and chlorobenzene at room temperature, whereas **P3** was only sparingly soluble at room temperature, although its solubility in hot (ca. 80 °C) chlorobenzene or 1,2-dichlorobenzene was reasonable. All polymers afforded satisfactory elemental analysis and ^1H NMR spectra.

The polymers had moderate number-average molecular weights (M_n) as measured by gel permeation chromatography (GPC) in hot (80 °C) chlorobenzene (Table 1). The similar molecular weights and dispersities across the series allowed for a direct comparison of their properties. The thermal behavior of the polymers showed some differences across the series. Thus, **P3** exhibited no obvious thermal transitions by differential scanning calorimetry (DSC) upon heating to 250 °C, whereas **P1** and **P2** exhibited melt endotherms at 168 and 130 °C, respectively, which by analogy to pBTTT may be attributable to side-chain melt. There was no indication of a backbone melt up to 250 °C.

The UV−vis absorption spectra of **P1−P3** in dilute, room-temperature 1,2-dichlorobenzene and as thin films are shown in Figure 2. In solution, **P1** and **P2** exhibit similar spectral shapes, with absorption maxima at 497 and 503 nm, respectively. However, **P3** exhibits a substantially red-shifted spectrum, with a maximum at 552 nm and a shoulder at 585 nm. In films, **P1−P3** exhibit absorption maxima of 538, 553, and 586 nm, respectively. The 41, 50, and 34 nm red-shifts of the absorption peaks are indicative of backbone planarization and solid-state aggregation.

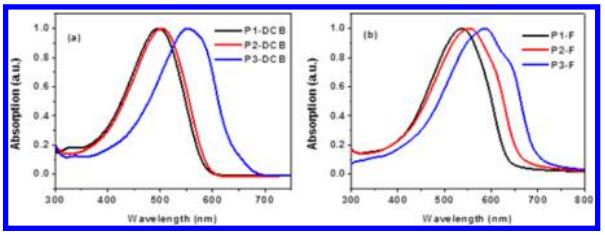

Figure 2. UV−vis spectra of **P1−P3** in dilute dichlorobenzene (a) and in thin films (b).

Polymer **P3** also exhibits a pronounced shoulder at 631 nm, with a less pronounced shoulder also observable for **P2**. Considering the only difference among the polymers is the regiochemistry of the side chains, this suggests that **P3** has the largest effective conjugation of the polymers. This is further supported by the optical band gaps measured from the absorption onsets of 1.97, 1.88, and 1.78 eV, and the thin-film ionization potentials of 5.11, 5.08, and 4.97 eV for **P1−P3**, respectively. Both sets of data suggest that **P3** has more effective delocalization along the backbone in the solid state.

To help explain the different physical properties among these polymers, density functional theory (DFT) calculations of trimers (i.e., three repeat units) of **P1−P3** were modeled using Gaussian 09 at the B3LYP/6-31G* level. The side chains were shortened to ethyl groups in order to simplify the calculations, while still maintaining some steric bulk. The minimum-energy conformations of the trimers (Figure S2) show that both **P1** and **P2** have significant torsional twisting of 30.5° and 31.3° between adjacent thiophene and thieno[3,2-*b*]thiophene units, mainly as a result of interactions between the ethyl groups and the sulfur orbitals. In contrast, **P3** adopts an almost completely co-planar backbone, with an angle of just 3.7° between the same two aromatics. In this instance the ethyl groups are adjacent to the vinyl bond, and no steric twisting occurs between these groups. The calculations indicate that **P1** and **P2** adopt twist conformations, while **P3** adopts a more planar conformation, which agrees with the longer conjugation length and higher solid-state aggregation. The calculations also predict that **P3** has the highest HOMO level (Table 1) among these polymers, which is consistent with the photoelectron spectroscopy in air (PESA) data.

FETs with top-gate, bottom-contact (TG-BC) device architecture were fabricated to investigate the charge carrier mobility of these polymers. All three polymers yield operational transistors from three annealing temperatures (T_a), 100, 150, and 200 °C, with excellent field-effect, on/off channel current ratios in the range of 10^4−10^5, negligible operating hysteresis, and good drain current saturation. Using the field-effect mobility as a performance metric, the polymers can be ranked in an increasing order of performance as **P1**, **P2**, and **P3**. Figure 3a shows the saturation mobility (μ_{sat}) of the three polymers for each annealing temperature in a box chart format. The box represents where 50% of the data lie, along with its median, while the cross

dx.doi.org/10.1021/ja508798s | J. Am. Chem. Soc. 2014, 136, 15154−15157

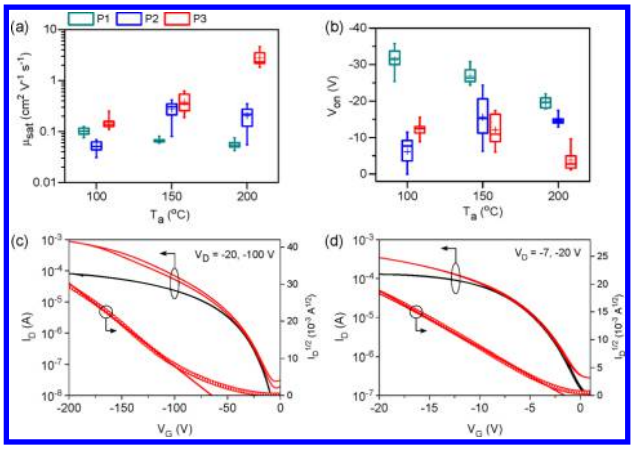

Figure 3. Dependence of (a) saturation mobility (μ_{sat}) and (b) onset voltage (V_{on}) on annealing temperature (T_a) for TG-BC thin-film transistors based on **P1** (dark cyan), **P2** (blue), and **P3** (red). The box chart indicates where 50% of the data lie, along with the median. The cross symbol denotes the mean average, and the whiskers the 5th and 95th percentiles. Representative set of transfer characteristics of a **P3**-based transistor (T_a = 200 °C) using CYTOP (c) or the high-k relaxor ferroelectric P(VDF-TrFE-CFE) (d) as a gate dielectric. The channel length and width are L = 40 μm and W = 1 mm, respectively, and the calculated hole mobility measured in saturation (μ_{sat}) is approximately 4.6 cm^2 V^{-1} s^{-1} for (c) and 1 cm^2 V^{-1} s^{-1} for (d).

denotes the mean average and the whiskers the 5th and 95th percentiles. For **P1**, the average value of μ_{sat} decreases with increasing annealing temperature, declining from 0.1 cm^2 V^{-1} s^{-1} for T_a = 100 °C to 0.05 cm^2 V^{-1} s^{-1} for T_a = 200 °C. **P2** shows an increase from 0.05 cm^2 V^{-1} s^{-1} for T_a = 100 °C to 0.3 cm^2 V^{-1} s^{-1} for T_a = 150 °C, before slightly decreasing to 0.2 cm^2 V^{-1} s^{-1} for T_a = 200 °C. However, devices based on **P3** exhibit an increase in the hole mobility from 0.2 to 0.4 cm^2 V^{-1} s^{-1} for T_a = 100 and 150 °C, respectively, followed by a significant increase to 2.8 cm^2 V^{-1} s^{-1} for T_a = 200 °C. The same trend can also be observed in the liner mobility (μ_{lin}) for all three polymers, although the values of μ_{lin} are consistently smaller than μ_{sat}.

Examining the subthreshold characteristics of the transistors, the trap densities calculated from the subthreshold swing for all cases do not exhibit a clear trend with T_a and are all in the range of (1−5) × 10^{12} eV^{-1} cm^{-2}. This suggests that the change in performance is not largely due to the change in trap states' distribution in energy within the semiconductors. However, the onset voltage (V_{on}), which is the gate voltage at which the subthreshold conduction begins, shows a dependency on T_a, as illustrated in Figure 3b. In particular, the V_{on} for the **P2** devices is found to shift toward more negative V_G, while in transistors based on **P1** and **P3**, the V_{on} moves closer to zero V_G with increasing T_a. This means that **P1**- and **P3**-based transistors require smaller gate electric fields to inject and accumulate holes into the semiconducting channel when annealed at higher temperatures, and vice versa for **P2**-based transistors. This shift in V_{on} might be related to the shift in the HOMO levels and/or the change in the deep trap states of the polymers upon annealing due to the evolution of the film morphology at the dielectric/semiconductor interface. However, more in-depth charge transport studies are required to clarify this behavior. Also, by comparing the **P1** and **P3** devices, the direction of change in V_{on} with T_a is not directly correlated to the change in the hole mobilities measured. The results from transistor characterization therefore seem to suggest that the origin of the high mobility obtained from **P3** devices annealed at 200 °C is not principally dependent on the electronic properties of the polymer, which is not unexpected, as all three polymers share the same backbone and are only different by the side chains. Further results reported hereinafter will give evidence that the side chains significantly affect the crystallinity of the polymers, which ultimately dictates the long-range hole-transport properties of these materials.

Figure 3c shows a representative set of the transfer characteristics of a high-performance **P3** transistor annealed at T_a = 200 °C. The average hole mobility extracted from these devices is μ_{sat} = 2.8(±1.0) cm^2 V^{-1} s^{-1}, with maximum values around 4.6 cm^2 V^{-1} s^{-1}. Noticeably, the devices are capable of conducting a rather high level of channel current which in some cases approaches 1 mA. Overall, the devices exhibit good transistor operation with negligible operating hysteresis, low V_{on}, and high channel current on/off ratio on the order of 10^5. In addition, noting that the operating voltage is rather high due to the low geometric capacitance (C_i) of the CYTOP dielectric layer (∼2.1 nF cm^{-2}) used for the devices, we realized low-voltage **P3**-based TG-BC transistors (T_a = 200 °C) using the high-k relaxor ferroelectric polymer dielectric poly(vinylidene fluoride-trifluoroethylene-chlorofluoroethylene) [P(VDF-TrFE-CFE) at 56/36.5/7.5 mol%] instead of CYTOP.[12] The resulting P(VDF-TrFE-CFE)-based transistors show operating characteristics similar to those of the CYTOP-based devices but are fully operational within the V_G range of 0 to −20 V (Figure 3d). Despite the low-voltage operation, the transistors are also capable of delivering drain currents in the 0.1−1 mA range, with an average hole mobility of 1 cm^2 V^{-1} s^{-1}. The slightly lower mobility value is most likely due to the non-optimized process followed during the fabrication of these low-voltage transistors and/or due to the rather different electrostatic nature of the high-k/polymer channel interface. Further work is currently underway to understand the origin of this difference.

To gain a better understanding of the effects of the alkyl chain's position and thermal annealing on the transistor performance, the film morphologies were investigated by grazing-incidence wide-angle X-ray scattering (GIWAXS) and atomic force microscopy (AFM) after coating and annealing under conditions identical to those used for the thin-film transistor measurements. The 2D WAXS patterns of **P1** and **P2** are shown in Figure S6, and that for **P3** is shown in Figure 4. For **P1** and **P2**, the films both appear to pack in a lamellar-like fashion with a mainly edge-on orientation and a (100) spacing of 2.4 and 2.0 nm, respectively, after annealing at 100 °C. Films annealed at 150 °C are similar to those annealed at 100 °C, whereas annealing at 200 °C, well above the apparent side-chain melt observed in DSC, results in a loss of most of the diffraction peaks, and the patterns become dominated by an amorphous halo. AFM topography images (Figures S7 and S8) show that root-mean-square surface roughness decreases upon annealing at 200 °C, which might be expected for less crystalline films. **P3** also packs in an edge-on lamellar fashion, with a (100) spacing of 1.9 nm, but unlike **P1** and **P2**, it also shows well-defined π-stacking (010) peaks in the charge-transport direction. In contrast to **P1** and **P2**, thermal annealing above 100 °C increases the diffraction intensity of the **P3** films, with the film annealed at 200 °C showing a strong increase in the number of orders of lamellar reflection. The AFM images show no reduction of film roughness upon annealing and retain an isotropic nodule-like structure throughout. However, there is no indication of the formation of large-scale molecular terraces as seen in pBTTT.[6] The 150 and

dx.doi.org/10.1021/ja508798s | J. Am. Chem. Soc. 2014, 136, 15154−15157

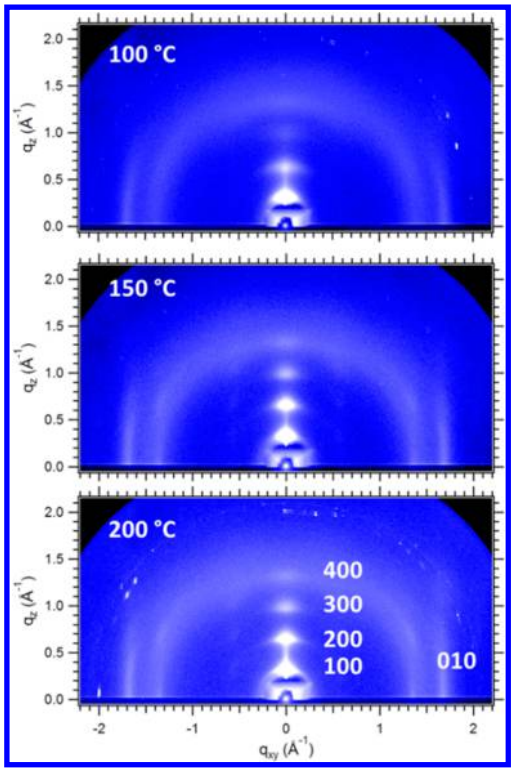

Figure 4. GIXD detector images of **P3** after annealing at 100, 150, and 200 °C.

200 °C annealed **P3** films both show evidence for three-dimensional order in the diffraction patterns.

The increase in thin-film order for **P3** upon annealing correlates reasonably with the significant improvement in transistor performance observed, particularly upon annealing at 200 °C, although it is somewhat surprising that **P1** and **P2** maintain reasonable FET performance at this temperature, considering the loss of thin-film order. High-temperature annealing is known to improve transistor performance in many cases,[1,2,13] possibly as a result of the elimination of traps or improved physical contact with the electrodes, and we suggest that for **P1** and **P2** this improvement is offset by the loss of order of the film. The side-chain ordering of **P3** increases aggregation and melting point, and the film is able to maintain order, even during high-temperature annealing.

In conclusion, we have demonstrated that the regiochemistry of the side chains has a significant impact on the optoelectronic properties and propensity to aggregate for a series of isomeric polythiophenes. On the basis of DFT calculations, we relate this to differences in torsional disorder along the polymer backbone. The polymer with the lowest degree of conformational disorder shows the longest effective conjugation length and demonstrates excellent performance in field-effect transistors, with peak mobilities up to 4.6 $cm^2 V^{-1} s^{-1}$.

■ ASSOCIATED CONTENT

Supporting Information

Experimental procedures, transistor plots, and AFM and DSC images, including Scheme S1 and Figures S1−S14. This material is available free of charge via the Internet at http://pubs.acs.org.

■ AUTHOR INFORMATION

Corresponding Author

m.heeney@imperial.ac.uk

Notes

The authors declare no competing financial interest.

■ ACKNOWLEDGMENTS

This work was support by EPSRC (EP/G060738/1). Portions of this research were carried out at the Stanford Synchrotron Radiation Lightsource, a Directorate of SLAC National Accelerator Laboratory and an Office of Science User Facility operated for the U.S. Department of Energy Office of Science by Stanford University.

■ REFERENCES

(1) (a) Kang, I.; Yun, H.-J.; Chung, D. S.; Kwon, S.-K.; Kim, Y.-H. *J. Am. Chem. Soc.* **2013**, *135*, 14896. (b) Kim, G.; Kang, S.-J.; Dutta, G. K.; Han, Y.-K.; Shin, T. J.; Noh, Y.-Y.; Yang, C. *J. Am. Chem. Soc.* **2014**, *136*, 9477. (c) Li, J.; Zhao, Y.; Tan, H. S.; Guo, Y.; Di, C.-A.; Yu, G.; Liu, Y.; Lin, M.; Lim, S. H.; Zhou, Y.; Su, H.; Ong, B. S. *Sci. Rep.* **2012**, *2*, 754.

(2) (a) Tseng, H.-R.; Phan, H.; Luo, C.; Wang, M.; Perez, L. A.; Patel, S. N.; Ying, L.; Kramer, E. J.; Nguyen, T.-Q.; Bazan, G. C.; Heeger, A. J. *Adv. Mater.* **2014**, *26*, 2993. (b) Tseng, H.-R.; Ying, L.; Hsu, B. B. Y.; Perez, L. A.; Takacs, C. J.; Bazan, G. C.; Heeger, A. J. *Nano Lett.* **2012**, *12*, 6353. (c) Luo, C.; Kyaw, A. K. K.; Perez, L. A.; Patel, S.; Wang, M.; Grimm, B.; Bazan, G. C.; Kramer, E. J.; Heeger, A. J. *Nano Lett.* **2014**, *14*, 2764.

(3) Yuen, J. D.; Wudl, F. *Energy Environ. Sci.* **2013**, *6*, 392.

(4) Biniek, L.; Schroeder, B. C.; Nielsen, C. B.; McCulloch, I. *J. Mater. Chem.* **2012**, *22*, 14803.

(5) Sirringhaus, H. *Adv. Mater.* **2014**, *26*, 1319.

(6) McCulloch, I.; Heeney, M.; Bailey, C.; Genevicius, K.; MacDonald, I.; Shkunov, M.; Sparrowe, D.; Tierney, S.; Wagner, R.; Zhang, W.; Chabinyc, M. L.; Kline, R. J.; McGehee, M. D.; Toney, M. F. *Nat. Mater.* **2006**, *5*, 328.

(7) Ong, B. S.; Wu, Y.; Liu, P.; Gardner, S. *J. Am. Chem. Soc.* **2004**, *126*, 3378.

(8) Chabinyc, M. L.; Toney, M. F.; Kline, R. J.; McCulloch, I.; Heeney, M. *J. Am. Chem. Soc.* **2007**, *129*, 3226.

(9) Noriega, R.; Rivnay, J.; Vandewal, K.; Koch, F. P. V.; Stingelin, N.; Smith, P.; Toney, M. F.; Salleo, A. *Nat. Mater.* **2013**, *12*, 1038.

(10) Zhang, X.; Bronstein, H.; Kronemeijer, A. J.; Smith, J.; Kim, Y.; Kline, R. J.; Richter, L. J.; Anthopoulos, T. D.; Sirringhaus, H.; Song, K.; Heeney, M.; Zhang, W.; McCulloch, I.; DeLongchamp, D. M. *Nat. Commun.* **2013**, *4*, 2238.

(11) (a) Chen, G.-Y.; Cheng, Y.-H.; Chou, Y.-J.; Su, M.-S.; Chen, C.-M.; Wei, K.-H. *Chem. Commun.* **2011**, *47*, 5064. (b) He, Y.; Wu, W.; Zhao, G.; Liu, Y.; Li, Y. *Macromolecules* **2008**, *41*, 9760. (c) Zhang, X.; Koehler, M.; Matzger, A. J. *Macromolecules* **2004**, *37*, 6306. (d) Li, Y. N.; Wu, Y. L.; Liu, P.; Birau, M.; Pan, H. L.; Ong, B. S. *Adv. Mater.* **2006**, *18*, 3029.

(12) (a) Li, J.; Sun, Z.; Yan, F. *Adv. Mater.* **2012**, *24*, 88. (b) Pattanasattayavong, P.; Yaacobi-Gross, N.; Zhao, K.; Ndjawa, G. O. N.; Li, J.; Yan, F.; O'Regan, B. C.; Amassian, A.; Anthopoulos, T. D. *Adv. Mater.* **2013**, *25*, 1504.

(13) Park, S.; Lim, B. T.; Kim, B.; Son, H. J.; Chung, D. S. *Sci. Rep.* **2014**, *4*, 5482.